

# Supplementary Material: Order-Adaptive and Illumination-Aware Variational Optical Flow Refinement

Daniel Maurer  
maurer@vis.uni-stuttgart.de

Michael Stoll  
stoll@vis.uni-stuttgart.de

Andrés Bruhn  
bruhn@vis.uni-stuttgart.de

Institute for Visualization and  
Interactive Systems  
University of Stuttgart, Germany

## 1 Details on the Minimisation

As stated in the main paper, we apply the well-known coarse-to-fine warping strategy, which is based on a hierarchical incremental formulation with two nested fixed point iterations [1]. The outer fixed point iteration approximates the original energy functional as a series of differential energies. Starting from a coarse scale initialisation, it thereby successively refines the solution  $\mathbf{w}^k$ ,  $\mathbf{c}^k$ ,  $\mathbf{a}^k$ ,  $\mathbf{b}^k$  from a coarser scale  $k$  via

$$\mathbf{w}^{k+1} = \mathbf{w}^k + \mathbf{d}\mathbf{w}^k, \quad (1)$$

$$\mathbf{c}^{k+1} = \mathbf{c}^k + \mathbf{d}\mathbf{c}^k, \quad (2)$$

$$\mathbf{a}^{k+1} = \mathbf{a}^k + \mathbf{d}\mathbf{a}^k, \quad (3)$$

$$\mathbf{b}^{k+1} = \mathbf{b}^k + \mathbf{d}\mathbf{b}^k, \quad (4)$$

using the increments  $\mathbf{d}\mathbf{w}^k$ ,  $\mathbf{d}\mathbf{c}^k$ ,  $\mathbf{d}\mathbf{a}^k$ ,  $\mathbf{d}\mathbf{b}^k$  computed on the next finer scale  $k+1$ . Thereby, the ratio between two consecutive resolution levels is given by  $\eta \in (0, 1]$ . Please note that, in contrast to all other functions, the spatially varying order weight  $o^k$  is not estimated incrementally. As shown in [5] it can be computed in closed form at each resolution level.

While the general strategy resembles the standard coarse-to-fine scheme used by many variational methods, it is important to note that our reduced coarse-to-fine scheme does not start at a very coarse level and a zero initial guess. Instead it begins the refinement at an intermediate level, where it can benefit from the results of the preceding pipeline (matching, outlier filtering, inpainting) in terms of good initialisation. This strategy also differs significantly from those of other refinement methods that only refine the initialisation at the finest level, i.e. at the original resolution. Such methods, however, are not able to correct large errors, since they easily get trapped in local minima close to the fine-grid initialisation.

**Differential Energy.** Let us now detail on the differential energy that has to be minimised at each resolution level to obtain the desired increments. It is given by

$$E_{\text{oir}}^k(\mathbf{dw}^k, \mathbf{dc}^k, o^k) = \int_{\Omega} D_{\text{illum}}^k(\mathbf{dw}^k, \mathbf{dc}^k) + \alpha \cdot R_{\text{oar}}^k(\mathbf{dw}^k, o^k) + \beta \cdot R_{\text{illum}}^k(\mathbf{dc}^k) + \gamma \cdot S_{\text{oar}}^k(o^k) d\mathbf{x}, \quad (5)$$

where the different terms from the original energy have been replaced by the corresponding differential formulations. In case of the data term the differential formulation reads

$$\begin{aligned} D_{\text{illum}}^k(\mathbf{dw}^k, \mathbf{dc}^k) = & \Psi_c \left( \boldsymbol{\theta} \cdot \left( f_x^k du^k + f_y^k dv^k + f^k - \Phi(g, \mathbf{c}^k + \mathbf{dc}^k) \right)^2 \right) \\ & + \lambda \cdot \Psi_c \left( \boldsymbol{\theta}_x \cdot \left( f_{xx}^k du^k + f_{xy}^k dv^k + f_x^k - \partial_x \Phi(g, \mathbf{c}^k) \right)^2 \right. \\ & \left. + \boldsymbol{\theta}_y \cdot \left( f_{yx}^k du^k + f_{yy}^k dv^k + f_y^k - \partial_y \Phi(g, \mathbf{c}^k) \right)^2 \right), \quad (6) \end{aligned}$$

where  $f^k = f(\mathbf{x} + \mathbf{w}^k)$  denotes the second frame  $f$  compensated by the current motion estimate  $\mathbf{w}^k$ . To keep the minimisation feasible we rely on a lagged computation of the coefficients within the gradient constancy and hence only use the coefficient increment  $\mathbf{dc}^k$  in the brightness constancy; see [9].

In contrast to the data term, the differential formulations of the remaining terms are straightforward. The regularisation term for the illumination coefficients is given by

$$R_{\text{illum}}^k(\mathbf{dc}^k) = \sum_{m=1}^2 \Psi_m \left( \sum_{n=1}^N \left( \mathbf{r}_m^\top \nabla (c_n^k + dc_n^k) \right)^2 \right), \quad (7)$$

the flow regulariser reads

$$\begin{aligned} R_{\text{oar}}^k(\mathbf{dw}^k, o^k) = & \inf_{\mathbf{da}^k, \mathbf{db}^k} \left\{ \bar{\sigma}^k \cdot S_1^k(\mathbf{dw}^k) \right. \\ & \left. + (1 - \bar{\sigma}^k) \cdot (S_2^k(\mathbf{dw}^k, \mathbf{da}^k, \mathbf{db}^k) + T) + \delta \cdot S_3^k(\mathbf{da}^k, \mathbf{db}^k) \right\}, \quad (8) \end{aligned}$$

with

$$\bar{\sigma}^k(\mathbf{x}) = \frac{1}{|\mathcal{N}(\mathbf{x})|} \int_{\mathcal{N}(\mathbf{x})} o^k(\mathbf{y}) d\mathbf{y}, \quad (9)$$

$$S_1^k(\mathbf{dw}^k) = \sum_{m=1}^2 \Psi_m \left( \left( \mathbf{r}_m^\top \nabla (u^k + du^k) \right)^2 + \left( \mathbf{r}_m^\top \nabla (v^k + dv^k) \right)^2 \right), \quad (10)$$

$$\begin{aligned} S_2^k(\mathbf{dw}^k, \mathbf{da}^k, \mathbf{db}^k) = & \sum_{m=1}^2 \Psi_m \left( \left( \mathbf{r}_m^\top \left( \nabla (u^k + du^k) - (\mathbf{a}^k + \mathbf{da}^k) \right) \right)^2 \right. \\ & \left. + \left( \mathbf{r}_m^\top \left( \nabla (v^k + dv^k) - (\mathbf{b}^k + \mathbf{db}^k) \right) \right)^2 \right), \quad (11) \end{aligned}$$

$$S_3^k(\mathbf{da}^k, \mathbf{db}^k) = \sum_{m=1}^2 \Psi_m \left( \sum_{l=1}^2 \left( \mathbf{r}_l^\top \mathcal{J}(\mathbf{a}^k + \mathbf{da}^k) \mathbf{r}_m \right)^2 + \left( \mathbf{r}_l^\top \mathcal{J}(\mathbf{b}^k + \mathbf{db}^k) \mathbf{r}_m \right)^2 \right), \quad (12)$$

and the selection term yields

$$S_{\text{oar}}(o^k) = \ln(1 - o^k) - o^k \cdot \ln \left( \frac{1}{o^k} - 1 \right). \quad (13)$$

**Euler-Lagrange Equations.** In order to minimise the differential energy (5) we solve the corresponding system of Euler-Lagrange equations, which form the necessary conditions for each minimiser [9]. By introducing the following abbreviations for the outer derivatives of the penaliser functions

$$\Psi'_{c,\text{bca}}{}^k := \Psi'_c \left( \boldsymbol{\theta} \cdot \left( f_x^k du^k + f_y^k dv^k + f^k - \Phi(g, \mathbf{c}^k + \mathbf{d}\mathbf{c}^k) \right)^2 \right), \quad (14)$$

$$\begin{aligned} \Psi'_{c,\text{gca}}{}^k := & \Psi'_c \left( \boldsymbol{\theta}_x \cdot \left( f_{xx}^k du^k + f_{xy}^k dv^k + f_x^k - \partial_x \Phi(g, \mathbf{c}^k) \right)^2 \right. \\ & \left. + \boldsymbol{\theta}_y \cdot \left( f_{yx}^k du^k + f_{yy}^k dv^k + f_y^k - \partial_y \Phi(g, \mathbf{c}^k) \right)^2 \right), \end{aligned} \quad (15)$$

$$\Psi'_{m,\text{illum}}{}^k := \Psi'_m \left( \sum_{n=1}^N \left( \mathbf{r}_m^\top \nabla (c_n^k + dc_n^k) \right)^2 \right), \quad (16)$$

$$\Psi'_{m,\text{S}_1}{}^k := \Psi'_m \left( \left( \mathbf{r}_m^\top \nabla (u^k + du^k) \right)^2 + \left( \mathbf{r}_m^\top \nabla (v^k + dv^k) \right)^2 \right), \quad (17)$$

$$\begin{aligned} \Psi'_{m,\text{S}_2}{}^k := & \Psi'_m \left( \left( \mathbf{r}_m^\top \left( \nabla (u^k + du^k) - (\mathbf{a}^k + \mathbf{d}\mathbf{a}^k) \right) \right)^2 \right. \\ & \left. + \left( \mathbf{r}_m^\top \left( \nabla (v^k + dv^k) - (\mathbf{b}^k + \mathbf{d}\mathbf{b}^k) \right) \right)^2 \right), \end{aligned} \quad (18)$$

$$\Psi'_{m,\text{S}_3}{}^k := \Psi'_m \left( \sum_{l=1}^2 \left( \mathbf{r}_l^\top \mathcal{J}(\mathbf{a}^k + \mathbf{d}\mathbf{a}^k) \mathbf{r}_m \right)^2 + \left( \mathbf{r}_l^\top \mathcal{J}(\mathbf{b}^k + \mathbf{d}\mathbf{b}^k) \mathbf{r}_m \right)^2 \right), \quad (19)$$

where the derivatives of the penaliser functions themselves are given by

$$\Psi'_1(s^2) = \frac{1}{1 + s^2/\varepsilon^2}, \quad (20)$$

$$\Psi'_c(s^2) = \Psi'_2(s^2) = \frac{1}{\sqrt{1 + s^2/\varepsilon^2}}, \quad (21)$$

as well as by introducing the following four diffusion tensors

$$\mathbf{T}_{\text{illum}}^k = \sum_{m=1}^2 \Psi'_{m,\text{illum}}{}^k \cdot \mathbf{r}_m \mathbf{r}_m^\top, \quad (22)$$

$$\mathbf{T}_{\text{S}_1}^k = \sum_{m=1}^2 \Psi'_{m,\text{S}_1}{}^k \cdot \mathbf{r}_m \mathbf{r}_m^\top, \quad (23)$$

$$\mathbf{T}_{\text{S}_2}^k = \sum_{m=1}^2 \Psi'_{m,\text{S}_2}{}^k \cdot \mathbf{r}_m \mathbf{r}_m^\top, \quad (24)$$

$$\mathbf{T}_{\text{S}_3}^k = \sum_{m=1}^2 \Psi'_{m,\text{S}_3}{}^k \cdot \mathbf{r}_m \mathbf{r}_m^\top, \quad (25)$$

we can write the resulting system of Euler-Lagrange equations as

$$\begin{aligned}
0 = \frac{\delta E_{\text{oir}}^k}{\delta du^k} &= \Psi'_{\text{c,bca}}{}^k \cdot \theta \cdot \left( f_x^k du^k + f_y^k dv^k + f^k - \Phi(g, \mathbf{c}^k + \mathbf{d}\mathbf{c}^k) \right) \cdot f_x^k \\
&\quad + \lambda \cdot \Psi'_{\text{c,gca}}{}^k \cdot \left( \theta_x \cdot \left( f_{xx}^k du^k + f_{xy}^k dv^k + f_x^k - \partial_x \Phi(g, \mathbf{c}^k) \right) \cdot f_{xx}^k \right. \\
&\quad \quad \left. + \theta_y \cdot \left( f_{yx}^k du^k + f_{yy}^k dv^k + f_y^k - \partial_y \Phi(g, \mathbf{c}^k) \right) \cdot f_{yx}^k \right) \\
&\quad - \alpha \cdot \bar{\sigma}^k \cdot \text{div} \left( \mathbf{T}_{\mathbf{S}_1}^k \nabla(u^k + du^k) \right) \\
&\quad - \alpha \cdot (1 - \bar{\sigma}^k) \cdot \text{div} \left( \mathbf{T}_{\mathbf{S}_2}^k \left( \nabla(u^k + du^k) - (\mathbf{a}^k + \mathbf{d}\mathbf{a}^k) \right) \right) \tag{26}
\end{aligned}$$

$$\begin{aligned}
0 = \frac{\delta E_{\text{oir}}^k}{\delta dv^k} &= \Psi'_{\text{c,bca}}{}^k \cdot \theta \cdot \left( f_x^k du^k + f_y^k dv^k + f^k - \Phi(g, \mathbf{c}^k + \mathbf{d}\mathbf{c}^k) \right) \cdot f_y^k \\
&\quad + \lambda \cdot \Psi'_{\text{c,gca}}{}^k \cdot \left( \theta_x \cdot \left( f_{xx}^k du^k + f_{xy}^k dv^k + f_x^k - \partial_x \Phi(g, \mathbf{c}^k) \right) \cdot f_{xy}^k \right. \\
&\quad \quad \left. + \theta_y \cdot \left( f_{yx}^k du^k + f_{yy}^k dv^k + f_y^k - \partial_y \Phi(g, \mathbf{c}^k) \right) \cdot f_{yy}^k \right) \\
&\quad - \alpha \cdot \bar{\sigma}^k \cdot \text{div} \left( \mathbf{T}_{\mathbf{S}_1}^k \nabla(v^k + dv^k) \right) \\
&\quad - \alpha \cdot (1 - \bar{\sigma}^k) \cdot \text{div} \left( \mathbf{T}_{\mathbf{S}_2}^k \left( \nabla(v^k + dv^k) - (\mathbf{b}^k + \mathbf{d}\mathbf{b}^k) \right) \right) \tag{27}
\end{aligned}$$

$$\begin{aligned}
\mathbf{0} = \frac{\delta E_{\text{oir}}^k}{\delta \mathbf{d}\mathbf{c}^k} &= \Psi'_{\text{c,bca}}{}^k \cdot \theta \cdot \left( f_x^k du^k + f_y^k dv^k + f^k - \Phi(g, \mathbf{c}^k + \mathbf{d}\mathbf{c}^k) \right) \cdot (\phi_1(g), \phi_2(g))^\top \\
&\quad - \beta \cdot \mathbf{div} \left( \mathcal{J}(\mathbf{c}^k + \mathbf{d}\mathbf{c}^k) \mathbf{T}_{\text{illum}}^k \right) \tag{28}
\end{aligned}$$

$$\mathbf{0} = \frac{\delta E_{\text{oir}}^k}{\delta \mathbf{d}\mathbf{a}^k} = (1 - \bar{\sigma}^k) \cdot \mathbf{T}_{\mathbf{S}_2}^k \left( (\mathbf{a}^k + \mathbf{d}\mathbf{a}^k) - \nabla(u^k + du^k) \right) - \delta \cdot \mathbf{div} \left( \mathcal{J}(\mathbf{a}^k + \mathbf{d}\mathbf{a}^k) \mathbf{T}_{\mathbf{S}_3}^k \right) \tag{29}$$

$$\mathbf{0} = \frac{\delta E_{\text{oir}}^k}{\delta \mathbf{d}\mathbf{b}^k} = (1 - \bar{\sigma}^k) \cdot \mathbf{T}_{\mathbf{S}_2}^k \left( (\mathbf{b}^k + \mathbf{d}\mathbf{b}^k) - \nabla(v^k + dv^k) \right) - \delta \cdot \mathbf{div} \left( \mathcal{J}(\mathbf{b}^k + \mathbf{d}\mathbf{b}^k) \mathbf{T}_{\mathbf{S}_3}^k \right) \tag{30}$$

$$0 = \frac{\delta E_{\text{oir}}^k}{\delta \sigma^k} \Rightarrow \sigma^k = \frac{1}{1 + e^{-\xi/\gamma}} \quad \text{with} \quad \xi = \int_{\mathcal{N}(\mathbf{x})} \frac{1}{|\mathcal{N}(\mathbf{y})|} \left( T + S_2^k - S_1^k \right) dy. \tag{31}$$

Here  $\frac{\delta E_{\text{oir}}^k}{\delta *}$  with  $* \in \{du^k, dv^k, \mathbf{d}\mathbf{c}^k, \mathbf{d}\mathbf{a}^k, \mathbf{d}\mathbf{b}^k, \sigma^k\}$  denote functional derivatives of  $E_{\text{oir}}^k$ , and  $\mathbf{div}$  is the extension of the divergence operator to matrix-valued functions, which applies the standard divergence operator to each row of the function.

**Numerical Solution.** In order to solve the system of Euler-Lagrange equations (26)-(31) we discretise them using standard finite differences in case of the data term related expressions and non-standard approximations in case of the divergence expressions [8]. This leads to a non-linear system of equations due to the outer derivatives  $\Psi'_{\text{c,bca}}{}^k$ ,  $\Psi'_{\text{c,gca}}{}^k$ ,  $\Psi'_{m,\text{illum}}{}^k$ ,  $\Psi'_{m,\mathbf{S}_1}{}^k$ ,  $\Psi'_{m,\mathbf{S}_2}{}^k$ ,  $\Psi'_{m,\mathbf{S}_3}{}^k$  of the sub-quadratic penaliser functions. To cope with this non-linear system of equations a second (inner) fixed point iteration is applied and the particular non-linear contributions are kept fixed to obtain a linear system of equations. Finally, we apply a cascadic multicolour variant of the SOR method to solve this linear system of equations.

## 2 Additional Results

In the Figures 1-6 we provide additional qualitative results for sequences of the utilised benchmarks, namely KITTI 2012 [1], KITTI 2015 [2] and MPI Sintel [3]. To emphasise some aspects of our novel refinement strategy we highlighted certain regions in the images. Figure 1 and 2, for example, nicely show the benefit of the proposed reduced coarse-to-fine scheme, which allows to correct errors. Figure 3 and 6 bring out the adaptation to the underlying image structure, as seen at traffic lights and the ear of the villain. Finally, the benefit of the order adaptive regularisation not only becomes present in the boundary areas of the KITTI sequences (Figures 1-4) but also at the shoulder of Sintel in Figure 5.

## References

- [1] T. Brox, A. Bruhn, N. Papenberg, and J. Weickert. High accuracy optical flow estimation based on a theory for warping. In *Proc. European Conference on Computer Vision*, pages 25–36, 2004.
- [2] D. J. Butler, J. Wulff, G. B. Stanley, and M. J. Black. A naturalistic open source movie for optical flow evaluation. In *Proc. European Conference on Computer Vision*, pages 611–625, 2012.
- [3] O. Demetz. *Feature invariance versus change estimation in variational motion estimation*. PhD thesis, Saarland University, 2015.
- [4] A. Geiger, P. Lenz, and R. Urtasun. Are we ready for autonomous driving? the KITTI vision benchmark suite. In *In Proc. IEEE Conference on Computer Vision and Pattern Recognition*, pages 3354–3361, 2012.
- [5] I. M. Gelfand and S. V. Fomin. *Calculus of variations*. Dover Publications, 2000.
- [6] D. Maurer, M. Stoll, and A. Bruhn. Order-adaptive regularisation for variational optical flow: Global, local and in between. In *Proc. International Conference on Scale Space and Variational Methods in Computer Vision*, pages 550–562, 2017.
- [7] M. Menze and A. Geiger. Object scene flow for autonomous vehicles. In *Proc. IEEE Conference on Computer Vision and Pattern Recognition*, pages 3061–3070, 2015.
- [8] J. Weickert, M. Welk, and M. Wickert.  $L^2$ -stable nonstandard finite differences for anisotropic diffusion. In *Proc. International Conference on Scale Space and Variational Methods in Computer Vision*, pages 380–391, 2013.

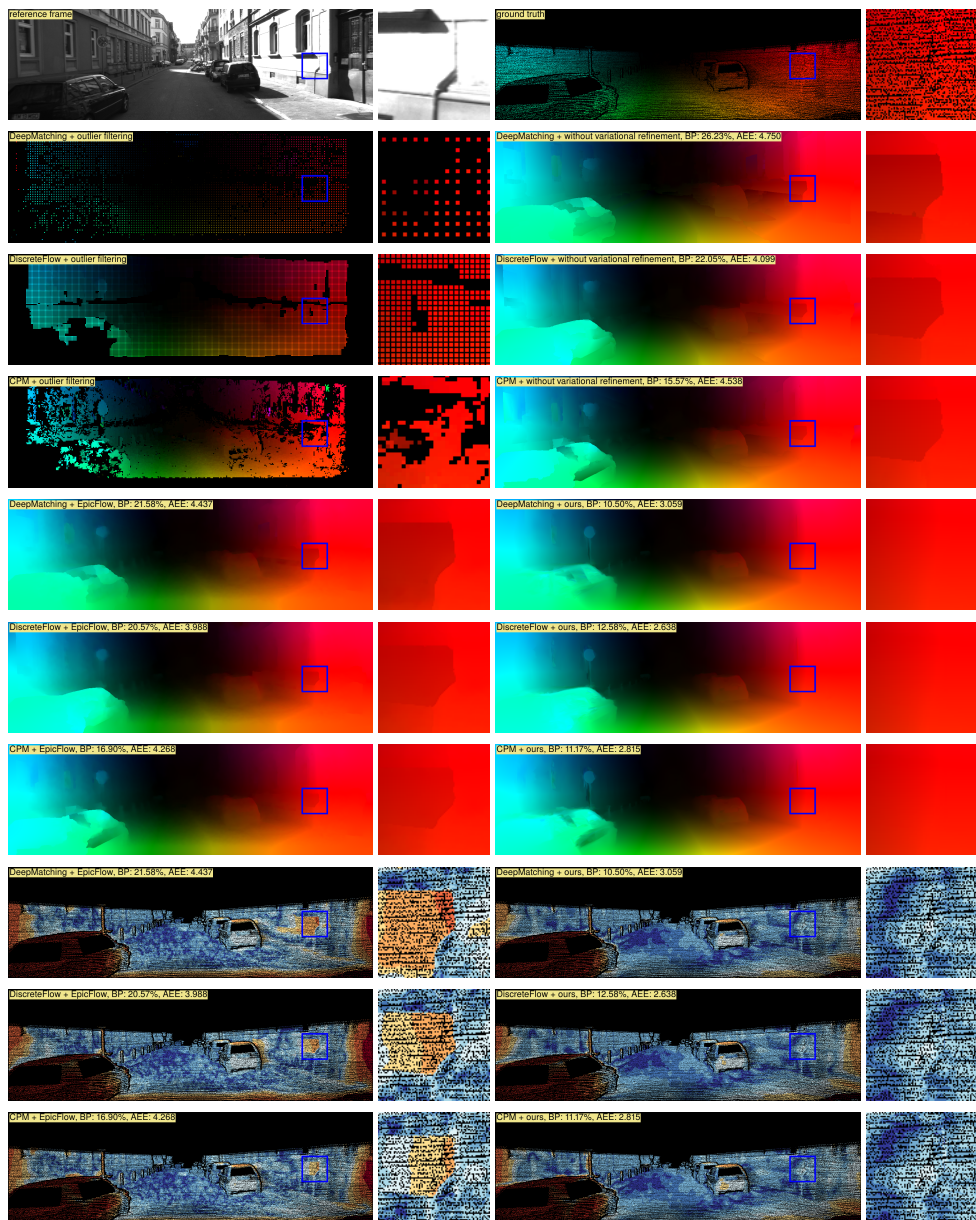


Figure 1: Results for the sequence #15 of the KITTI 2012 benchmark [1]. **Top to bottom:** Reference frame and ground truth. DeepMatching matches, DiscreteFlow matches, CPM matches (repetitive). **Second to fourth row:** Outlier-filtered matches and inpainted matches. **Fifth to seventh row:** Flow field visualisation of the EpicFlow refinement and proposed refinement. **Eighth to tenth row:** Bad pixel visualisation (3px threshold) of the EpicFlow refinement and proposed refinement.

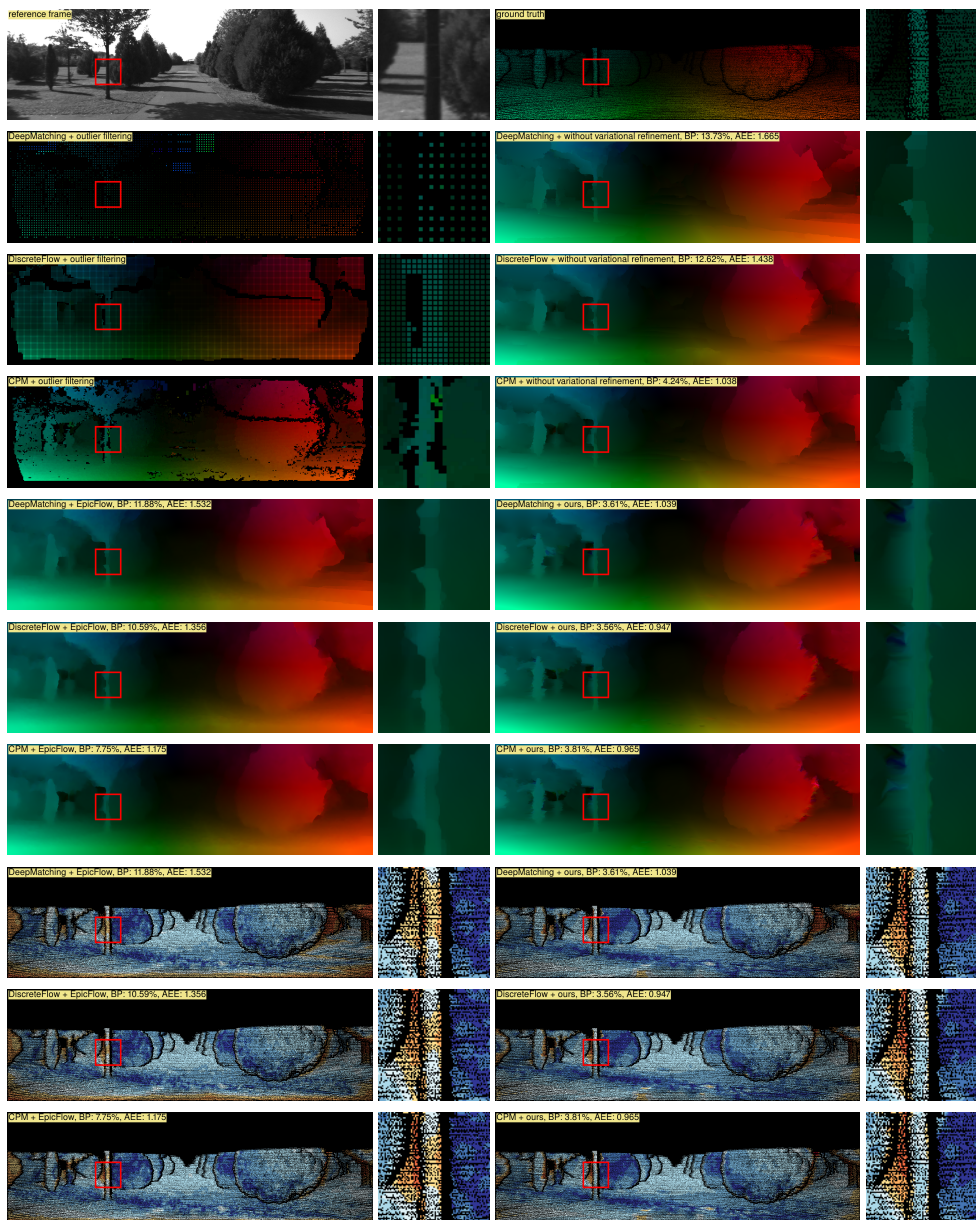


Figure 2: Results for the sequence #9 of the KITTI 2012 benchmark [1]. **Top to bottom:** Reference frame and ground truth. DeepMatching matches, DiscreteFlow matches, CPM matches (repetitive). **Second to fourth row:** Outlier-filtered matches and inpainted matches. **Fifth to seventh row:** Flow field visualisation of the EpicFlow refinement and proposed refinement. **Eighth to tenth row:** Bad pixel visualisation (3px threshold) of the EpicFlow refinement and proposed refinement.

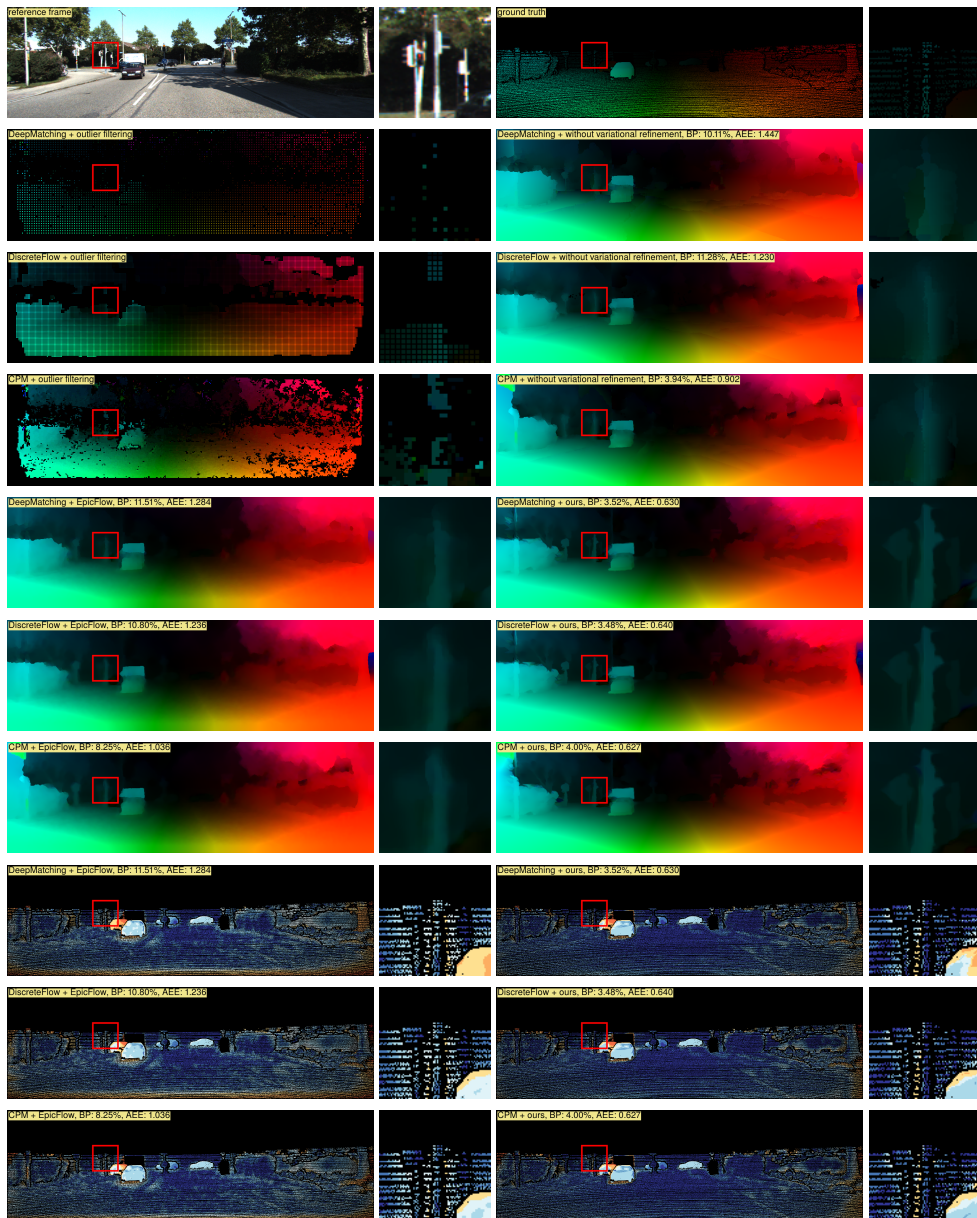


Figure 3: Results for the sequence #07 of the KITTI 2015 benchmark [1]. **Top to bottom:** Reference frame and ground truth. DeepMatching matches, DiscreteFlow matches, CPM matches (repetitive). **Second to fourth row:** Outlier-filtered matches and inpainted matches. **Fifth to seventh row:** Flow field visualisation of the EpicFlow refinement and proposed refinement. **Eighth to tenth row:** Bad pixel visualisation (3px threshold) of the EpicFlow refinement and proposed refinement.

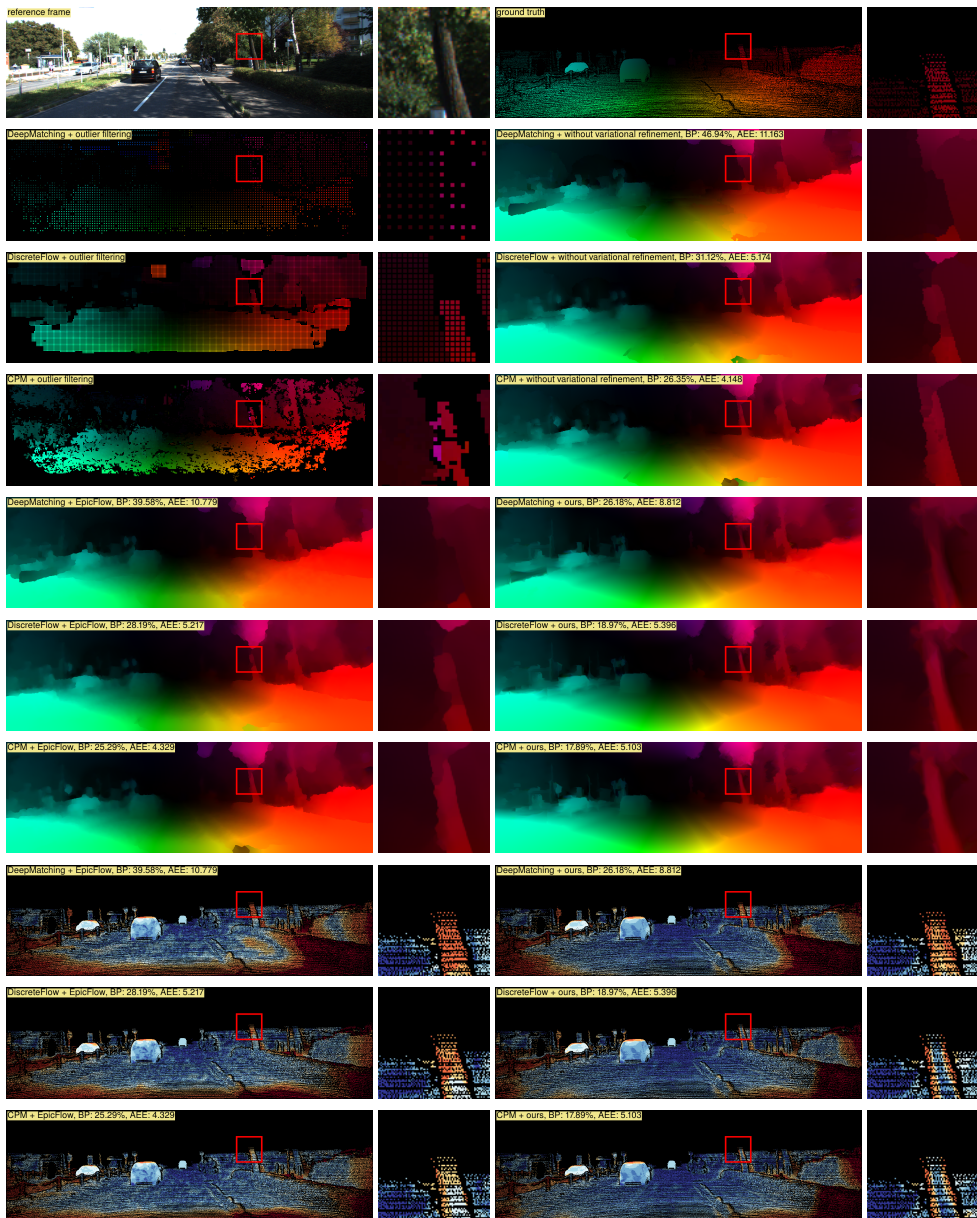


Figure 4: Results for the sequence #31 of the KITTI 2015 benchmark [1]. **Top to bottom:** Reference frame and ground truth. DeepMatching matches, DiscreteFlow matches, CPM matches (repetitive). **Second to fourth row:** Outlier-filtered matches and inpainted matches. **Fifth to seventh row:** Flow field visualisation of the EpicFlow refinement and proposed refinement. **Eighth to tenth row:** Bad pixel visualisation (3px threshold) of the EpicFlow refinement and proposed refinement.

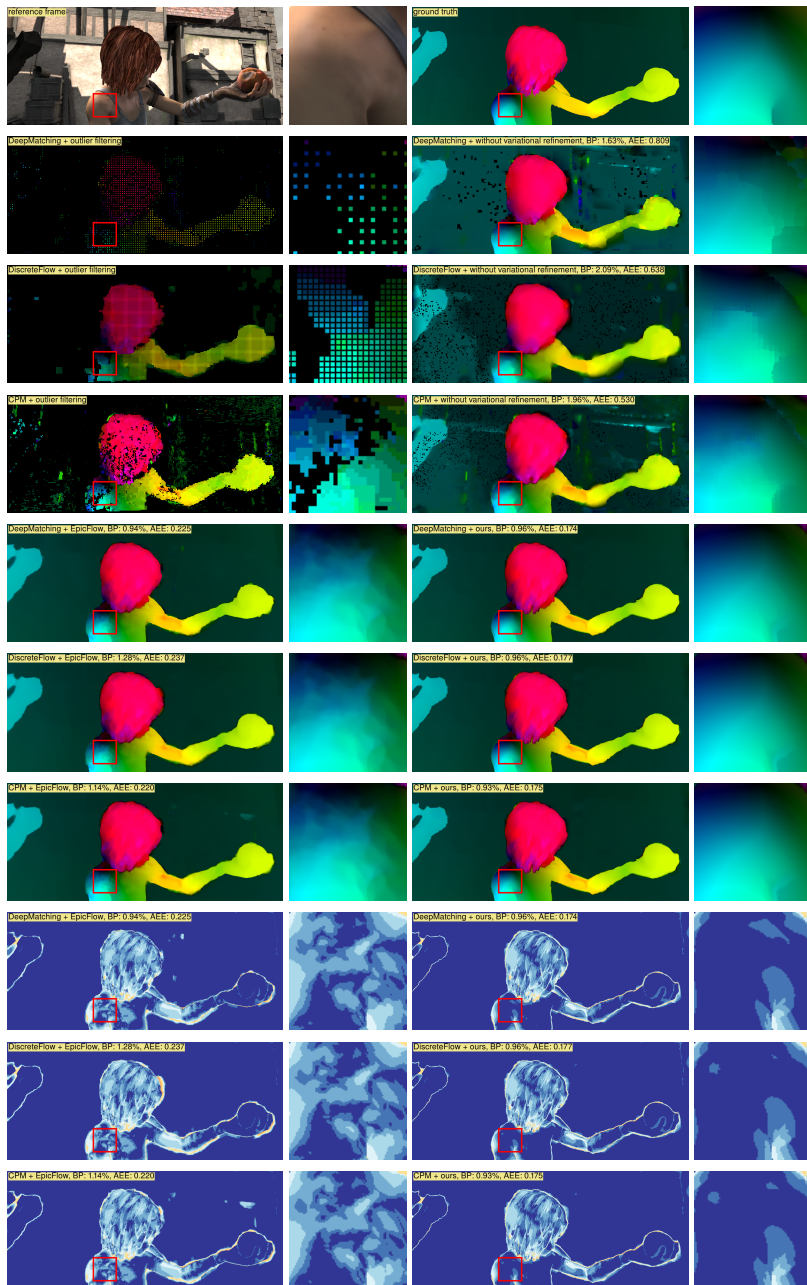


Figure 5: Results for sequence #20 (alley\_1) of the MPI Sintel benchmark [1]. **Top to bottom:** Reference frame and ground truth. DeepMatching matches, DiscreteFlow matches, CPM matches (repetitive). **Second to fourth row:** Outlier-filtered matches and inpainted matches. **Fifth to seventh row:** Flow field visualisation of the EpicFlow refinement and proposed refinement. **Eighth to tenth row:** Bad pixel visualisation (3px threshold) of the EpicFlow refinement and proposed refinement.

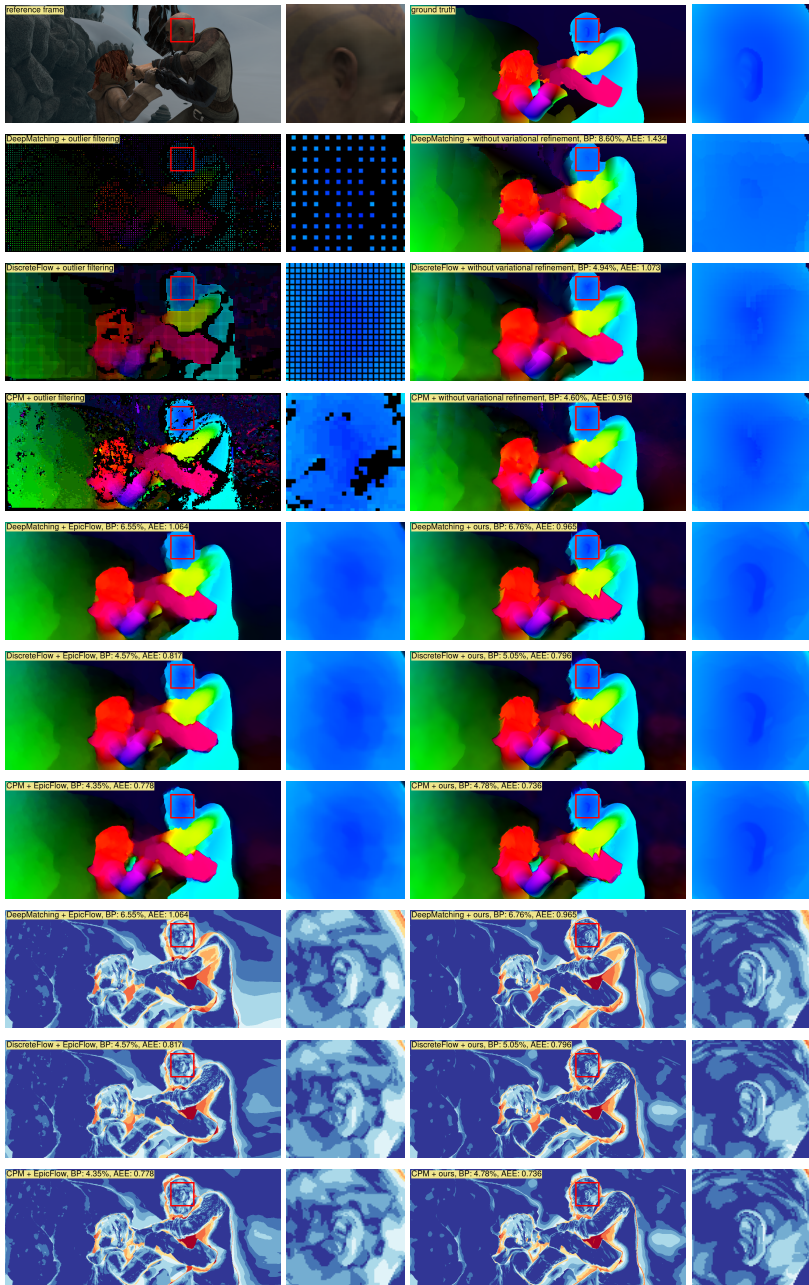


Figure 6: Results for sequence #02 (ambush\_5) of the MPI Sintel benchmark [1]. **Top to bottom:** Reference frame and ground truth. DeepMatching matches, DiscreteFlow matches, CPM matches (repetitive). **Second to fourth row:** Outlier-filtered matches and inpainted matches. **Fifth to seventh row:** Flow field visualisation of the EpicFlow refinement and proposed refinement. **Eighth to tenth row:** Bad pixel visualisation (3px threshold) of the EpicFlow refinement and proposed refinement.